~~A new conceptual model reveals a long ramp-like change as cause for~~ Simulating global ice volume across the Mid-Pleistocene Transition with a ramp-like increase in the deglaciation threshold

Felix Pollak[1,2,5], Frédéric Parrenin[1], Émilie Capron[1], Zanna Chase[2,3], Lenneke Jong[4,5], and Etienne Legrain[6,7]

[1]Université Grenoble Alpes, CNRS, INRAE, IRD, Grenoble INP, IGE, Grenoble, France
[2]Institute for Marine and Antarctic Studies, University of Tasmania, Hobart, TAS, Australia
[3]Australian Research Council Centre for Excellence in Antarctic Science (ACEAS), University of Tasmania, Hobart, TAS, Australia
[4]Australian Antarctic Division, Department of Climate Change, Energy, the Environment and Water, Kingston, TAS, Australia
[5]Australian Antarctic Program Partnership, Institute for Marine and Antarctic Studies, University of Tasmania, Hobart, TAS, Australia
[6]Laboratoire de Glaciologie, Université libre de Bruxelles, Brussels, Belgium
[7]Department of Water and Climate, Vrije Universiteit Brussel, Brussels, Belgium

Correspondence: Felix Pollak (felix.pollak@univ-grenoble-alpes.fr)

Abstract. During the Quaternary period, spanning the last 2.6 million years, the characteristic frequency and amplitude of glacial-interglacial cycles evolved from low-amplitude 41,000-year cycles to high-amplitude 100,000-year cycles. This transition occurred around 1.2 to 0.8 million years ago and is referred to as the Mid-Pleistocene Transition (MPT). The absence of any significant change in the external orbital forcing during this period suggests the existence of some fundamental change within the Earth-climate system, leading to non-linearities or feedback mechanisms. The temporal structure of such a change is still under debate. Here, we present a new conceptual model of the Quaternary global climate, the so-called RAMP model. ~~It can be applied to different paleoclimatic records and variables as the global mean sea level, benthic foraminifera $\delta^{18}O$ and seawater $\delta^{18}O_{sw}$,~~ which can reconstruct the past global ice volume. The RAMP model incorporates a ramp-like change in its deglaciation threshold to reconstruct the MPT. Parameter optimization finds that the onset of the change occurs in the early Quaternary (2.6 - ~~2.2~~ 2.3 Ma) and lasts into the 100 kyr world (~~500~~ 550 - 250 ka). These findings support the idea of a long-term shift as a cause of the MPT and imply that the climate shift began early in the Quaternary. The model uses a linear combination of ~~precession~~ the precession parameter and obliquity as external orbital forcing, which can be optimized to best reconstruct the target ~~paleoclimatic record~~ curve. The identified orbital forcing differs from the widely used insolation at summer solstice at 65° N, as it exhibits a larger precession signal. ~~While the~~ The RAMP model yields consistent and good results for two different global mean sea level curves ~~and one benthic $\delta^{18}O$ record, it fails in reconstructing a recent deconvolution into seawater $\delta^{18}O_{sw}$, which significantly differs from the other curves~~. Moreover, we ~~perform various~~ conduct a series of sensitivity tests, in which the RAMP model demonstrates ~~high robustness, especially the identified long-term trend~~ strong robustness. In particular, the identified long-lasting period for the ramp is a very robust feature ~~in~~ of the model, ~~indicating its importance~~ underscoring its key role in reconstructing the MPT.

1

1 Introduction

The Quaternary is the most recent geological epoch, covering the last 2.6 Ma. It is characterized by the alternance of cold glacial climate states and warmer interglacial periods. In the first half of the 20th century, Milutin Milankovitch made significant contributions to the astronomical theory of climate, which links changes in Earth's orbital parameters to changes in the radiative forcing, which ultimately leads to glacial-interglacial variability (Milankovitch, 1941). Earth's obliquity varies on a cycle of approximately 41 kyr, while precession operates over a 19 kyr and a 23 kyr period, and eccentricity fluctuates on a 100 kyr and a 400 kyr timescale (Hays et al., 1976). In his theory, the orbital variations of Earth's eccentricity, obliquity and precession lead to variations in the insolation during boreal summer, which is the dominating driver of glacial cycles (Ganopolski, 2024).

Two central problems arise from this theory. The first is known as the 100 kyr problem: The late Quaternary glacial cycles (approximately the last 800 ka) follow 100 kyr patterns, despite the eccentricity having only a negligible influence on the global insolation compared to the obliquity and precession (Raymo and Huybers, 2008; Imbrie et al., 2011; Barker et al., 2022). The second issue is related to the shift of low-amplitude ~41 kyr cycles towards high-amplitude ~100 kyr cycles during the mid-Pleistocene (~1.2 - 0.8 Ma) in the absence of any significant change in orbital forcing. This transition is known as the Mid-Pleistocene Transition (MPT) (Imbrie et al., 2011; Barker and Knorr, 2023; Elderfield et al., 2012). The occurrence of the MPT poses one of the most challenging open questions to the paleoclimatological community and has been the subject of intense studies (Willeit et al., 2019; Legrain et al., 2023; Berends et al., 2021b; Ganopolski, 2024). Various internal feedback mechanisms of the climate system and non-linearities have been put forward to explain this major climatic shift (Legrain et al., 2023; Berends et al., 2021b).

Recent studies suggest that the duration and timing of deglaciation and glaciation events over the last 900 ka were largely deterministic and driven by the relative phasing of precession, obliquity, and eccentricity (Barker et al., 2022, 2025). Barker et al. (2025) identified candidate precession peaks, which are precession peaks that begin while obliquity is increasing, as essential for glacial terminations. They found that all glacial terminations during the last 900 ka correspond to the first candidate precession peak after a minimum in eccentricity. This is how the 100 kyr periodicity comes into play for the post-MPT world. On the other hand, it seems like obliquity alone controls the following glacial inception, which is triggered by the start of its next decreasing phase. During and prior to the MPT, the authors found that almost all candidate precession peaks are linked to glacial terminations. Since they depend on rising obliquity values, they are mainly paced by obliquity, resulting in the observed 41 kyr world with no more influence of eccentricity on these cycles. This leaves open the question of why there was a change in the climate response to candidate precession peaks.

While various hypotheses have been proposed to explain the MPT, the following two are particularly popular. The regolith hypothesis suggests that gradual removal of thick regolith layers (10-50 m) on the North American and Eurasian surface during continuous glaciations exposed the high-friction crystalline bedrock underneath, reducing basal ice flow and increasing ice sheet stability, leading to the observed 100 kyr periodicity (Clark and Pollard, 1998; Clark et al., 2006; Willeit et al., 2019). Alternatively, a gradual cooling trend, associated with a decrease in atmospheric CO_2 concentrations throughout the Quaternary, may have triggered the MPT (Scherrenberg et al., 2025). Based on such a long-term cooling trend, various feedback

mechanisms in the ice sheet or changes in the ocean circulations have been proposed as a secondary trigger for the MPT (Berends et al., 2021b).

Another open question concerns the temporal structure of the change that might have triggered the MPT. While a gradual scenario involves a linear change over the entire Quaternary (like the CO_2 hypothesis), a more abrupt scenario involves the crossing of some irreversible climatic thresholds over a short period of time (Legrain et al., 2023). One proposed abrupt mechanism involves non-linear feedback effects from the merging of the North American Laurentide and Cordilleran ice sheets (Berends et al., 2021b; Bintanja and van de Wal, 2008; Gregoire et al., 2012).

Moreover, the effects of the MPT on the evolution of global ice volume across the Quaternary remain incompletely understood, as there are currently two contrasting views. The reconstruction of global ice volume is based on benthic foraminifera $\delta^{18}O_b$, measured in marine records. It consists of two components, a temperature $\delta^{18}O_T$ and a seawater $\delta^{18}O_{sw}$ component, with the latter serving as a proxy for global ice volume. One common approach to disentangle these two components from the $\delta^{18}O_b$ signal is to apply some kind of regression method. This approach largely reproduces the variability present in the $\delta^{18}O_b$ signal, resulting in small ice sheets in the early Pleistocene, which increase in volume after the MPT. In contrast, a recent study by Clark et al. (2025b) deconvolved $\delta^{18}O_b$ into its seawater $\delta^{18}O_{sw}$ component, based on ocean temperature data, and subsequently Clark et al. (2025a) applied a mass-balance approach to this $\delta^{18}O_{sw}$ record, considering time-varying temperature and ice volume effects on the $\delta^{18}O$ of ice sheets, to reconstruct the Global Mean Sea Level (GMSL) over the past 4.5 Ma. This reconstruction no longer shows an increase in global ice volume over the Pleistocene, but just a transition in glacial frequency. Furthermore, this curve exhibits large ice sheets around 2.5 Ma, which is in better agreement with terrestrial (Balco and Rovey, 2010) and marine (Shakun et al., 2016; Rea et al., 2018) evidence. So at present, there are two fundamentally distinct perspectives on how global ice volume varied throughout the Pleistocene and on how the MPT affected the global ice volume variability.

Climate models present a versatile tool for investigating these different hypotheses and open questions. They range from computationally expensive Earth System Models to simple, zero-dimensional (spatial dimensions) conceptual models that focus on key variables while allowing long simulations. They rely on a reduced number of highly aggregated macroscopic variables that try to reconstruct the full dynamics as closely as possible (Saltzman, 2001). Various conceptual models have been developed over the last decades, varying in their underlying assumptions and hypotheses. Many of them yield good results and can reconstruct the 100 kyr world with its characteristic saw-tooth pattern (Gildor and Tziperman, 2001; Imbrie et al., 2011; Parrenin and Paillard, 2012; Pérez-Montero et al., 2024) or even the MPT with its shift in amplitude and frequency and its specific timing (Paillard, 1998; Paillard and Parrenin, 2004; Legrain et al., 2023; Ganopolski, 2024).

A common approach is to attribute glacial-interglacial variability to relaxation oscillations between multiple equilibria (Paillard, 1998; Parrenin and Paillard, 2012; Legrain et al., 2023; Leloup and Paillard, 2022). In his initial work, Paillard (1998) proposed a three-state model (hereafter referred to as P98) consisting of an interglacial, mild glacial, and a full glacial state. Transitions between model states depend on the ice volume and the insolation. To account for a change in forcing due to decreasing atmospheric CO_2 concentrations, he added a small linear trend in the radiative forcing and linearly increased one of the state thresholds. This model is able to accurately reconstruct the global ice volume over the past 2 Ma, with good results

in the timing of terminations and the change in periodicity due to the MPT. In later work, Parrenin and Paillard (2012) presented an improved version of this model (hereafter referred to as PP12), which only consists of a glaciation and a deglaciation ~~state~~regime. While the deglaciation trigger depends on a combination of ice volume and insolation, the glacial inception is solely controlled by insolation. Moreover, they adapted the solar forcing, such that the model takes a linear combination of three orbital parameters instead of a fixed insolation curve. A similar approach was used in the model of Imbrie et al. (2011). Indeed, the model results seem to depend on the chosen insolation forcing, since they differ in their contributions from obliquity and precession (Leloup and Paillard, 2022). The three model versions by Legrain et al. (2023) (hereafter referred to as L23 models) continued the work by implementing different internal forcing scenarios to test which of them is most likely to reproduce the MPT. In addition to the external solar forcing, they added internal variations to the model in the form of a varying deglaciation threshold. They found that a gradual increase of this deglaciation threshold is more likely to reproduce the MPT than an abrupt change. Based on this finding, they suggested that a gradual decline in atmospheric CO_2 concentrations over the Pleistocene may have increased the deglaciation threshold, potentially causing the MPT.

Imbrie et al. (2011) proposed a phase-space model that again combines ice volume and orbital forcing as a deglaciation trigger. They were able to reproduce the shift in frequency of glacial-interglacial cycles purely by orbital forcing, without changing any model parameters during the MPT. Hence, they linked the occurrence of 100 kyr glacial cycles to the eccentricity-driven amplitude modulation of precession. However, their model-data comparison was limited to a detrended benthic $\delta^{18}O$ curve rather than an ice volume reconstruction, thereby precluding the assessment of whether their model accurately reconstructs the change in amplitude over the MPT.

In a more recent work, Ganopolski (2024) attempted to set up a generalized Milankovitch Theory by incorporating model results from CLIMBER-2 (a more sophisticated Earth-System Model) into a conceptual model. The model can reproduce the glacial cycles of the Quaternary based on the nonlinear response of the climate system to the orbital forcing in the form of the eccentricity-driven amplitude modulation of precession and the existence of supercritical ice sheets. A gradual increase in the critical ice volume is added to model the MPT. The author associates this with the gradual removal of terrestrial sediments in the Northern Hemisphere (NH), which is needed to prolong the late-Pleistocene glacials.

In this study, we improve the 2-state L23 conceptual models. To account for potential feedback mechanisms in the climate system or internal changes in the system, we implement a new ramp-like scenario, called the RAMP model. Here, the focus lies on the general temporal structure of such a change, allowing for its physical interpretation. The RAMP model covers all three temporal scenarios discussed in the L23 models and is characterized by its easy adjustability. In comparison with the L23 models, it can be run on different time scales, be extrapolated into the future, ~~be run on different tuning targets and for different climatic variables (global mean sea level, $\delta^{18}O$), and it~~ reconstruct different global ice volume curves, and can be easily re-tuned for new parameterizations (e.g. allowing to test the effects of changes in the state thresholds, forcing, etc.).

2 Methods

2.1 RAMP model

The new RAMP model presents an improved version of the L23 models. In the following, the model formulation is described. A detailed description of the changes compared to the L23 models can be found in the Supplementary Information (SI Sec. 1). ~~While the L23 models were used to simulate the global ice volume and relied on the sea level reconstruction by Berends et al. (2021a) as a tuning target, the RAMP model can be applied to various targets, including benthic foraminifera and seawater δ^{18}O. Targets, other than global ice volume, are scaled to the Berends et al. (2021a) sea level, then solved for this unit space, before being rescaled to their initial units. This allows for consistent parameter units for all tuning targets and comparable orders of magnitude, and, therefore, to use a single model for various dimensional paleoclimatic records.~~

The RAMP model uses orbital forcing as an input to reconstruct ~~a paleoclimatic curve~~ the global ice volume over the Quaternary. Leloup and Paillard (2022) showed that the model outcome depends on the chosen insolation forcing, which differ in their precession and obliquity signals (e.g. summer solstice or caloric season at 65° N). ~~This poses a bias to the model by~~ Hence, selecting a specific insolation metric can pose a bias to the model, since this determines the strength of the precession and obliquity signals in the model. Some earlier models (Imbrie et al., 2011; Parrenin and Paillard, 2012; Legrain et al., 2023) use instead a linear combination of ~~precession,~~ the precession and co-precession parameters and obliquity, which can represent insolation at most latitudes and seasons (Imbrie et al., 2011). In the RAMP model, we only use a linear combination of ~~precession~~ the precession parameter and obliquity. We show that such a linear combination of only two orbital parameters can indeed accurately reconstruct various insolation curves (SI Sec. 4). The following orbital parameters (normalized and dimensionless) from La2004 orbital solution (Laskar et al., 2004) are used:

$$\text{Esi: Precession parameter} \sim e\sin(\omega), \tag{1}$$

$$\text{Ob: Obliquity} \sim \epsilon, \tag{2}$$

with ω the precession angle taken from the vernal equinox and e the eccentricity.

Hence, the global ice volume change per unit time in response to the orbital forcing $I(t)$ $(\text{m}\,\text{kyr}^{-1})$ is defined in the model ~~is defined~~ as:

$$I(t) = \alpha_{\text{Esi}}\text{Esi}(t) + \alpha_{\text{O}}\text{Ob}(t), \tag{3}$$

with the constant weights α_{Esi} and α_{O} $(\text{m}\,\text{kyr}^{-1})$. For brevity, we will refer to $I(t)$ simply as the orbital forcing from here on.

The model has two different ~~states~~ regimes, the glaciation ~~state~~ (**g**) and the deglaciation ~~state~~ regime (**d**). ~~Therefore, the paleoclimatic quantity~~ Depending on the current model regime, the global ice volume $v(t)$, given in meter sea level equivalent (m sl), is driven by two first-order differential equations~~, depending on the current model state~~:

$$\text{g}: \frac{\mathrm{d}v(t)}{\mathrm{d}t} = -I(t) + \alpha_g, \tag{4}$$

$$\text{d}: \frac{\mathrm{d}v(t)}{\mathrm{d}t} = -I(t) - \frac{v(t)}{\tau_{\text{d}}}, \tag{5}$$

5

where α_g (m kyr^{-1}) is a constant model parameter controlling the glacial rate of advance and τ_d (kyr) is the constant relaxation time, which controls the deglacial rate of retreat.

A state change from a glaciation to a deglaciation ($\mathbf{g}$) $\rightarrow$ ($\mathbf{d}$) occurs when a combination of the current ~~quantity~~ <u>ice volume</u> $v(t)$ and the orbital forcing exceeds a critical threshold:

155 (i) $\quad v(t) \cdot \tilde{I}(t) + v(t) > v_0(t) \qquad$ & $\qquad$ (ii) $\quad v(t) \cdot \tilde{I}(t) > v_1.$ $\hfill$ (6)

Vice versa, a transition from a deglaciation ~~state~~ to a glaciation state ($\mathbf{d}$) $\rightarrow$ ($\mathbf{g}$) occurs when:

(i) $\quad v(t) \cdot \tilde{I}(t) + v(t) < v_0(t) \qquad$ & $\qquad$ (ii) $\quad v(t) \cdot \tilde{I}(t) < v_1.$ $\hfill$ (7)

To account for the correct units, the threshold equations use the dimensionless orbital forcing $\tilde{I}(t) = \frac{I(t)}{[I]} \tilde{I}(t)$. The time-dependent deglaciation parameter is denoted as $v_0(t)$ (m), and v_1 (m) is another model threshold but constant in time. Supple-

160 mentary Figure S3 visualizes how these thresholds act in the RAMP model and how they initiate state changes and drive the dynamics of the model.

To simulate the MPT, the L23 models (and their earlier precursor models) introduced a temporal change in the deglaciation parameter $v_0(t)$, as orbital forcing alone was not capable of simulating the MPT in their model. In the RAMP model, this parameter is altered ramp-like, i.e. it changes linearly during a period bounded by t_1 and t_2 (~~ka~~<u>kyr</u>) and stays constant before

165 and after:

$$v_0(t) = \begin{cases} v_{0,1}, & \text{if } t < t_1 \\ v_{0,1} + \frac{v_{0,2} - v_{0,1}}{t_2 - t_1}(t - t_1), & \text{if } t_1 \leq t \leq t_2 \\ v_{0,2}, & \text{if } t_2 < t \end{cases} \qquad (8)$$

with $v_{0,1}$ (m) the constant value before the ramp and with $v_{0,2}$ (m) the constant value after the ramp. The time t is ~~conventionally given in paleo units (ka BP~~<u>given in physical units (kyr</u>). This implementation covers three special temporal scenarios, all included in the three model versions discussed in L23:

170

(i) if $v_{0,1} = v_{0,2}$: no change in the deglaciation parameter. RAMP is only externally forced by changes in orbital parameters (equivalent to ORB model in L23)

(ii) if $t_1 = t_2$: abrupt jump in $v_0(t)$ (equivalent to ABR model in L23)

175 ~~if $t_1 = 2.6$~~

(iii) <u>if $t_1 = -2.6$</u> Myr and $t_2 = 0$ Myr: gradual trend over entire simulation period (equivalent to GRAD model in L23)

6

Therefore, the new RAMP model is more flexible than any of the L23 models, and for a linear trend in v_0, it also gives information on when such a trend has started and ended. Tuning the RAMP model to some ~~paleoclimatic target curve~~ global ice volume reconstruction reveals the temporal evolution in $v_0(t)$, needed to ~~best reproduce this curve~~ reproduce this target curve best.

In contrast to the L23 models, the newly developed RAMP model demonstrates superior numerical efficiency, exhibiting a speedup by a factor of approximately 30, and it incorporates a more advanced tuning strategy (more details in SI Sec. 1). The gain in numerical efficiency in combination with a more refined tuning strategy allowed us to test various parameterizations involving modifications to the model forcing, the evolutionary equations, or the threshold equations (SI Tab. S4). These tests enabled us to investigate the influence of various parameters and to identify less important ones that could be excluded from the final model. During this process, we identified the necessity of scaling the orbital forcing I in the threshold equation in such a way that it has a similar magnitude to the ~~quantity~~ ice volume v. Consequently, this allowed for a reduction in the number of parameters in the model compared to the L23 models (by 2 to 4 fewer), while simultaneously covering a broader range of temporal scenarios and improving the performance of the model.

2.2 Tuning targets

The L23 model reconstructed the global ice volume over the past 2 Ma by using the ~~global mean sea level (GMSL)~~ GMSL reconstruction by Berends et al. (2021a) as a tuning target. In ~~contrast~~ addition to this target, the RAMP model is extended to include ~~four different paleoclimatic records, which allow reconstructing not only the global ice volume, but also benthic $\delta^{18}O_b$ and seawater $\delta^{18}O_{sw}$~~ the GMSL reconstruction by Rohling et al. (2022).

The Berends sea level data reconstructs the past 3.6 Ma, based on an inverse forward modelling approach that aims to disentangle the coupled signals of ice volume and ocean temperature, present in benthic $\delta^{18}O$ records (Berends et al., 2021a). It uses the LR04 stack of benthic $\delta^{18}O$ as forcing (Lisiecki and Raymo, 2005). We keep the Berends curve as a target for global ice volume in the RAMP model, but also include the GMSL reconstruction by Rohling et al. (2022) to have a second target curve. In contrast to Berends et al. (2021a), they used the process modelling approach by Rohling et al. (2021) to deconvolve the sea level signal from the LR04 stack. Despite their different approaches to reconstructing the GMSL signal from the LR04 stack, both produce curves in strong agreement with each other, with a mean offset of 3.3 m (Rohling et al., 2022). In the period before 2.6 Ma, the offset is greater. In general, the Berends ~~record~~ curve is smoother compared to the Rohling ~~record~~ curve, which arises from a stronger inertia in changes in the ice volume present in the Berends model (Rohling et al., 2022).

~~A most recent work by Clark et al. (2025b) deconvolved the Prob-stack (Ahn et al., 2017), a global mean benthic $\delta^{18}O_b$ stack, into its seawater $\delta^{18}O_{sw}$ component, based on ocean temperature data. The Prob-stack was corrected for a long-term increase in $\delta^{18}O_b$, possibly due to a combined effect of diagenesis and the carbonate ion effect. To account for other targets than GMSL, we include the benthic $\delta^{18}O_b$ Prob-stack (Ahn et al., 2017), as detrended by Clark et al. (2025b) and its seawater component $\delta^{18}O_{sw}$ as two further tuning targets for the RAMP model.~~

3 Results

3.1 RAMP model for Quaternary climate

Tuning the RAMP model to the ~~detrended Prob-stack results in a high correlation between both curves ($R = 0.86$) and an RMSE of 0.22~~ GSML reconstruction, either by Berends et al. (2021a) (Fig. 1a) or Rohling et al. (2022) (Fig. 1~~a). b), yields similar results. The obtained model-data correlation is high for both curves ($R = 0.86$ and $R = 0.85$). The ~~model selects a long-lasting increasing trend for the deglaciation parameter in order to reconstruct the target curve. This ramp-like change occurs around 2.2 Ma and lasts until around 500 ka in the model. Furthermore, the~~ RAMP model can ~~correctly~~ accurately identify an increase in the ~~amplitude of $\delta^{18}O_b$ cycles~~ ice volume amplitude after the MPT. Although some of the post-MPT interglacial peaks are too low in the reconstruction. ~~During the period~~ The simulated glacial peaks in the period 1.4 - 1 ~~Ma, the glacial peaks tend to be too low in the RAMP model. Comparing the frequency scalograms of the RAMP reconstruction and its target curve demonstrates close resemblance (Fig. 2a,e). Both curves have a strong ~41 kyr obliquity signal over the entire Quaternary and an emerging ~100 kyr period after around 1~~ Ma ~~. However, the RAMP reconstruction features some consistent precession signals over the entire simulation period, which are not visible in the benthic targetcurve.~~

~~The RAMP model (purple lines) tuned for four different tuning targets: (a) Prob-stack benthic $\delta^{18}O_b$ (Ahn et al., 2017) as detrended by Clark et al. (2025b), (b) Berends et al. (2021a) GMSL curve, (c) Rohling et al. (2022) GMSL curve, and (d) Clark et al. (2025b) seawater $\delta^{18}O_{sw}$. The vertical black lines indicate the start and endpoint of the ramp and the dotted black lines show the temporal evolution of the deglaciation threshold. The grey-shaded area highlights the classical perspective of where the MPT is located in time. MIS boundaries are given according to Lisiecki and Raymo (2005). Model extrapolations for the future 100 kyr are indicated by the yellow-shaded areas.~~

~~Frequency scalograms from the continuous wavelet transform for the RAMP model (panel (a)-(d)) and its corresponding tuning targets: (e) Prob-stack benthic $\delta^{18}O_b$ (Ahn et al., 2017) as detrended by Clark et al. (2025b), (f) Berends et al. (2021a) GMSL curve, (g) Rohling et al. (2022) GMSL curve, and (h) Clark et al. (2025b) seawater $\delta^{18}O_{sw}$. White contours denote significant regions above the red-noise (AR1) background at the 95% confidence level. Orbital frequencies of precession (~23 kyr), obliquity (~ 41 kyr) and eccentricity (~ 100 kyr) are marked by the red dotted lines.~~

~~Tuning the RAMP model to the GSML reconstruction, either by Berends et al. (2021a) (Fig. 1b) or Rohling et al. (2022) (Fig. 1c) yields similar results. The obtained model-data correlation is high for both curves ($R = 0.86$ and $R = 0.85$). A general bias of too low interglacial peaks for the post-MPT world remains for these targets. The simulated glacial peaks before the MPT persist in being underestimated, especially visible for the Rohling target, which shows larger glacial-interglacial variations during this period. While the temporal evolution of~~ are underestimated for the Rohling target. The "double" interglacial peaks during Marine Isotope Stage (MIS) 15 and MIS 7 are accurately reconstructed for both target curves. In both cases, the deglaciation parameter $v_0(t)$ increases over the Quaternary. The timing for the onset and end of the ramp differs between the two curves. While for the Berends target~~closely resembles the one obtained for the benthic target, it does differ for the Rohling GMSL target. For this target , the rampbegins~~, the ramp starts 2291 ka and ends 546 ka, the Rohling target results in a prolonged ramp, which starts almost immediately in the simulation ~~and lasts longer, extending until approximately 250~~

ka. The at 2596 ka and lasts until 252 ka. Hence, both targets require an extended ramp-like increase in $v_0(t)$ in order to capture the amplitude and frequency change associated with the MPT. Comparing the spectral analysis of both reconstructions

245 (Fig. 2b,c) exhibits the same general patterns as for the benthic target with a,b) with their respective target curves (Fig. 2c,d) demonstrates that the RAMP model can accurately simulate the frequency shift associated with the MPT. Prior to the MPT, a dominant obliquity signal is visible, an arising ~100 kyr signal around 1 Ma and a significant precession signal over the entire simulation period.

Using the seawater $\delta^{18}O_{sw}$ record from Clark et al. (2025b) affects the simulation the most (Fig. 1d). For this target, the

250 RAMP model demonstrates the least correlation ($R = 0.63$). In general, while the Berends and Rohling GMSL curves and the benthic $\delta^{18}O_b$ show a similar pattern over the Quaternary, characterized by lower glacial-interglacial amplitudes prior to the MPT and an increase in peak glacial values, the $\delta^{18}O_{sw}$ curve displays a fundamentally different picture. Here, the glacial-interglacial cycles exhibit much stronger variations in the early Quaternary, and certain of these glacial maxima are comparable in strength to the ones occurring in the late Quaternary. Furthermore, the increasing trend in glacial maxima,

255 apparent for both GMSL curves and the benthic record, is not visible for the seawater $\delta^{18}O_{sw}$. In contrast, it exhibits an increasing period between 2 - 1.5 Ma, followed by a decreasing periodin the interval 1.2 - 0.8 Ma. The RAMP model struggles to reconstruct these features. Overall, the glacial-interglacial variations are significantly smaller for the RAMP reconstruction. While the pre-MPT glacial extrema are too small, the post-MPT interglacials are too weak. The identified ramp is very limited in time and appears after the MPT in the interval 400 - 200 ka. Hence, it differs substantially from the long-lasting patterns

260 observed for the previous three targets. Moreover, the RAMP model fails in reconstructing the post-MPT 100 kyr cycles (Fig. 2d) correctly. It only features a 100 kyr signal for the last ~200 kyr, after the ramp-like change in $v_0(t)$.

The tuned parameter values are very similar for the two GMSL targets and the detrended Prob-stack both GMSL target curves (SI Tab. S3). This highlights that the RAMP model , as discussed above, yields robust outputs for these three different tuning targets. While the $\delta^{18}O_{sw}$ target differs more significantly in its parameter values, certain parameters like $\alpha_{Esi}, \alpha_O, \alpha_g$

265 and $v_{0,1}$ remain similar.

Extrapolating the RAMP model 100 kyr into the future yields consistent results for all four tuning targets. For the Berends and Rohling GMSL curves and the detrended Prob-stack, the RAMP model simulates the end of the Holocene at both curves. The next glaciation threshold is crossed for both curves 6 ka and the subsequent glacial cycle to reach reaches its maximum at 64 kyr in the future. The $\delta^{18}O_{sw}$ target results in almost the same timings with an endpoint for the Holocene at 10 ka and a next

270 glacial maximum at 63 kyr in the future. For all four targets, the RAMP model underestimates the current interglacial lowstands Holocene minimum in global ice volume for both curves and projects an intermediate, strong future glaciation, compared to the previous onesglacial cycles.

The extended simulation period and the different tuning targets prevent a direct comparison between the RAMP and the L23 models. Hence, we run the RAMP model for a reduced simulation period of 2 Myr and tune it to the Berends GMSL

275 curve. A comparison with the GRAD model, which is the best-performing model version of L23, demonstrates better model-data agreement with a reduction in RMSE of more than 1 m, while relying on three parameters less, but still providing more

9
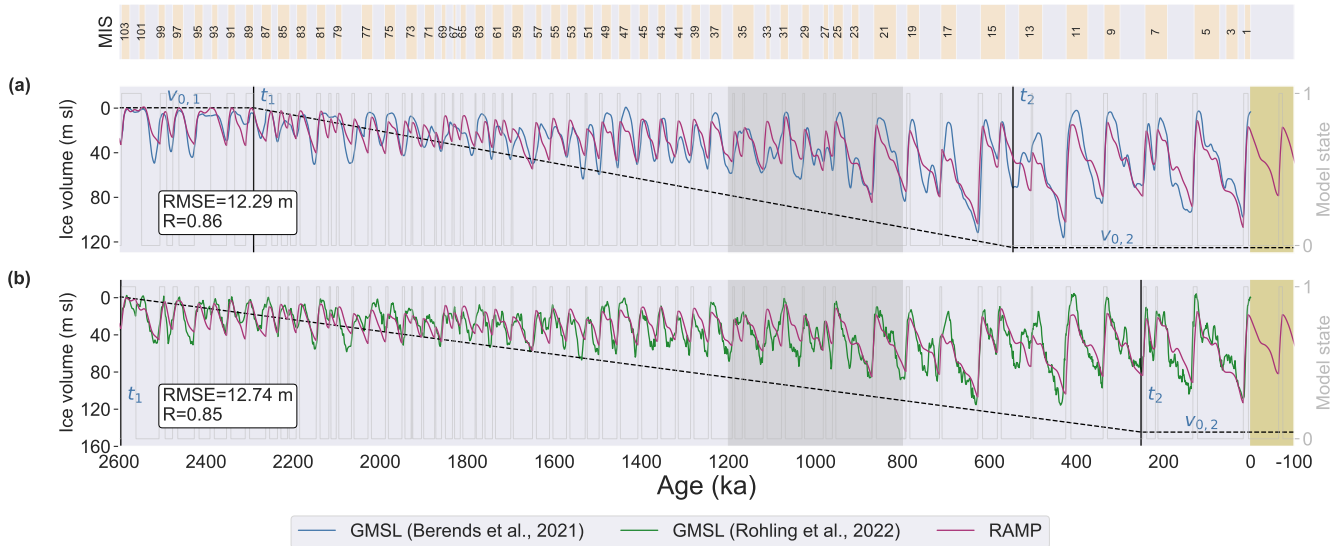
Figure 1. The RAMP model (purple lines) tuned for the two different tuning targets: **(a)** Berends et al. (2021a) GMSL curve and **(b)** Rohling et al. (2022) GMSL curve. The vertical black lines indicate the start and endpoint of the ramp and the dotted black lines show the temporal evolution of the deglaciation threshold. The grey-shaded area highlights the classical perspective of where the MPT is located in time. MIS boundaries are given according to Lisiecki and Raymo (2005). Model extrapolations for the future 100 kyr are indicated by the yellow-shaded areas.

information on the temporal change in $v_0(t)$. A complete comparison with all L23 model versions and the new RAMP model is shown in the SI (Fig. S1, Tab. S2).

3.2 Orbital forcing in the RAMP model

The temporal evolution of the ~~quantity~~ global ice volume $v(t)$ in the RAMP model is externally driven by the orbital forcing $I(t)$. It is based on a linear combination of the precession parameter and obliquity (Eq. 3). The two associated tunable model weights α_{Esi} and α_{O} determine how the orbital forcing in the RAMP model looks and how strong the precession and obliquity signals are. Figure 3 shows the resulting orbital forcings for the RAMP model, when tuned for each of the ~~four different~~ two tuning targets. To identify the insolation curve corresponding to the obtained $I(t)$ curve, we compare it to daily insolation curves at specific latitudes, monthly averaged ones, and various integrated summer insolations (ISI) [1]. The insolation values are taken from La2004 orbital solution (Laskar et al., 2004). Insolation curves and orbital forcing in the RAMP model are normalized for comparison.

---

[1] The integrated summer insolation (ISI) was introduced by Huybers (2006) and is defined as the sum of insolations on days exceeding some threshold τ:

$$\text{ISI}(\tau) = 86,400 \cdot \sum_i \beta_i W_i,$$

where W_i is the mean insolation in W/m^2 on day i, and $\beta_i = 1$ if $W_i \geq \tau$ and 0 otherwise.
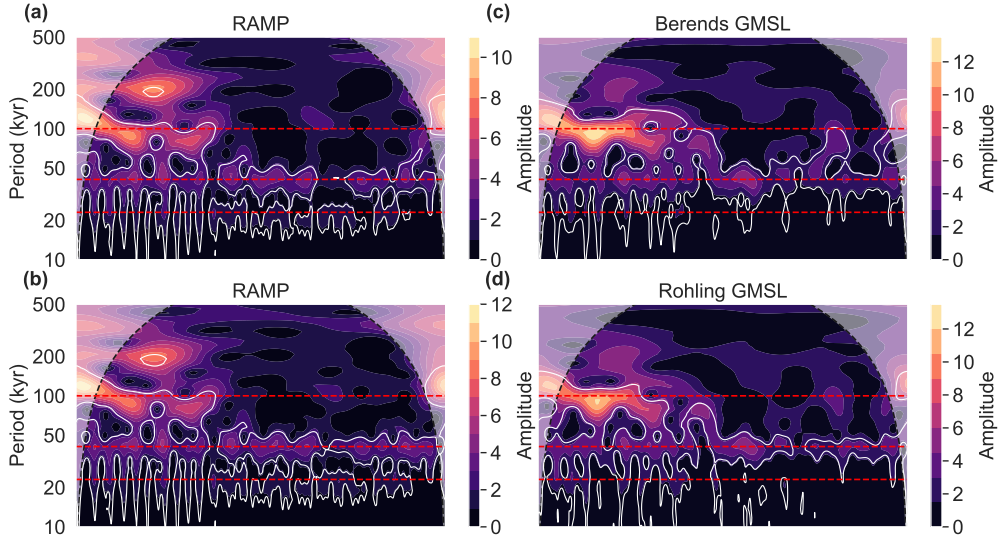
Figure 2. Frequency scalograms from the continuous wavelet transform for the RAMP model **(a)**, **(b)** and its corresponding tuning targets: **(c)** Berends et al. (2021a) GMSL curve and **(d)** Rohling et al. (2022) GMSL curve. White contours denote significant regions above the red-noise (AR1) background at the 95% confidence level. Orbital frequencies of precession (~23 kyr), obliquity (~41 kyr) and eccentricity (~100 kyr) are marked by the red dotted lines.
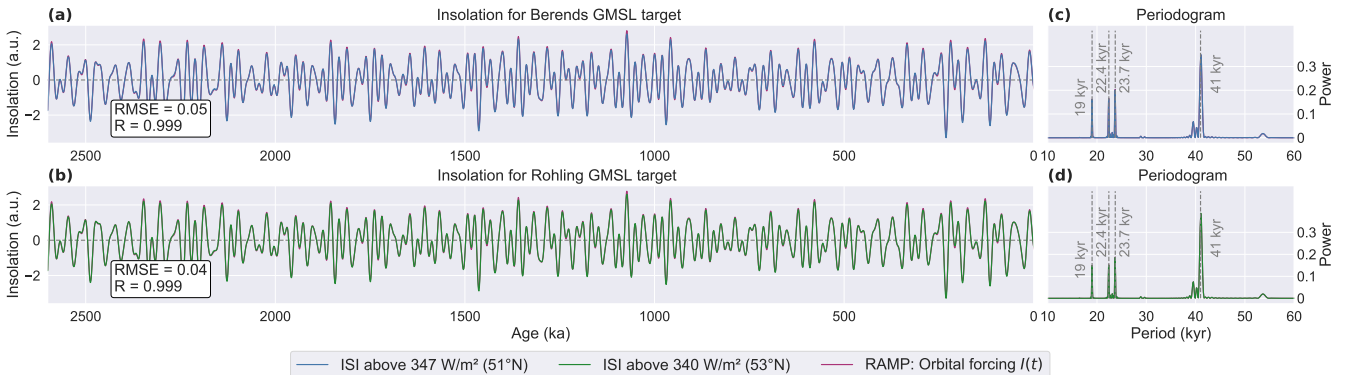
Figure 3. Comparison of the orbital forcing in the RAMP model (purple line), when tuned for the **(a)** ~~Prob-stack (Ahn et al., 2017) as detrended by Clark et al. (2025b), (b)~~ Berends et al. (2021a) GMSL reconstruction, ~~(c)~~ or the **(b)** Rohling et al. (2022) GMSL reconstruction~~and (d) Clark et al. (2025b) $\delta^{18}O_{sw}$ decomposition~~. For each forcing curve, the best-fitting insolation curve is shown. ISI curves were calculated by code from Leloup and Paillard (2022). ~~The RAMP model was tuned to the detrended Prob-stack.~~ Panel ~~(e)-(h)~~ **(c)** and **(d)** show the corresponding ~~periodogram~~ periodograms of both forcing curves.

The tuned weights ($\alpha_{\mathrm{Esi}}, \alpha_{\mathrm{O}}$) for the orbital forcing in the RAMP model exhibit ~~a remarkable similarity across all four~~ large similarity for both targets (SI Tab. S3). Consequently, it is unsurprising that the obtained orbital forcings for these targets closely

resemble one another, leading to a similar identification of the insolation curves with the highest correlation (Fig. 3a,b). For the Berends GMSL target, the closest correlation ($R = 0.999$) is found with the ISI above a threshold of 347 W m^{-2} at 51° N, and for the Rohling GMSL target, the closest correlation ($R = 0.999$) is found with the ISI above a threshold of 340 W m^{-2} at 53° N. The spectral analysis (Fig. 3c,d) of these insolation curves demonstrates that they consist of a dominant obliquity peak around 41 kyr, accompanied by pronounced precession peaks occurring around 19 kyr, 22.4 kyr and 23.7 kyr.

3.3 Model sensitivity

We conduct several experiments to assess the sensitivity of the RAMP model to initial conditions, the robustness of the glacial patterns to changes in model parameters and simulation time and how robust the model tuning is. Since both GMSL targets result in very similar outputs, we investigate the model sensitivity for the RAMP model when tuned for the Berends GMSL. We use the optimal parameter set (SI Tab. S3) for the RAMP model, keeping all parameters fixed except one. The first parameter that we vary, v_i, sets the initial ice volume for $v(t)$ (Fig. 4a). Lower initial values of 0%, 50%, 90% and 95% of the optimal value converge to the same output in less than 200 kyr. Similarly, higher values of 105%, 110%, 200% and 1000% converge to the same output in less than 200 kyr. This demonstrates that the RAMP model is not sensitive to the choice of initial ice volume.

The second parameter that we vary is the model threshold v_1, which we alter in an interval of $\pm10\%$ ($[0.9, 0.95, 1, 1.05, 1.1] \cdot v_{1,\text{best}}$) (Fig. 4b). There is almost no change in the simulated glacial cycles prior to the MPT. During the MPT, MIS 28 and 29 are affected by the altered model threshold. After the MPT, the interglacial double peak during MIS 7 seems to be most sensitive to this parameter change, and failing to detect this accurately can lead to an error propagation and an early termination of the last glacial period.

The last sensitivity test we perform concerns the deglaciation threshold $v_0(t)$. Here, we simultaneously vary $v_{0,1}$ and $v_{0,2}$ in an interval of $\pm10\%$ ($[0.9, 0.95, 1, 1.05, 1.1] \cdot v_{0,1/2,\text{best}}$) (Fig. 4c). This produces similar results as for the sensitivity test of v_1, although the model results are more sensitive to changes in $v_0(t)$ than to changes in v_1. Pre-MPT cycles are almost not affected by these changes. During the MPT, MIS 29 and 30 are again affected, as well as MIS 35. Glacial cycles after the MPT are most sensitive to parameter changes. Simulating the interglacial double peak during MIS 7 is again problematic. Furthermore, MIS 17 and MIS 13 are sensitive to changes in $v_0(t)$.

To assess the robustness of the model tuning, the RAMP model is tuned from a unit vector (i.e. initial parameter guess of 1 for all parameters) to the Berends GMSL curve, excluding the time interval from 2 to 0.6 Ma from the target dataset. Consequently, the RAMP model is only tuned for the early Quaternary (2.6 - 2 Ma) and the late Quaternary
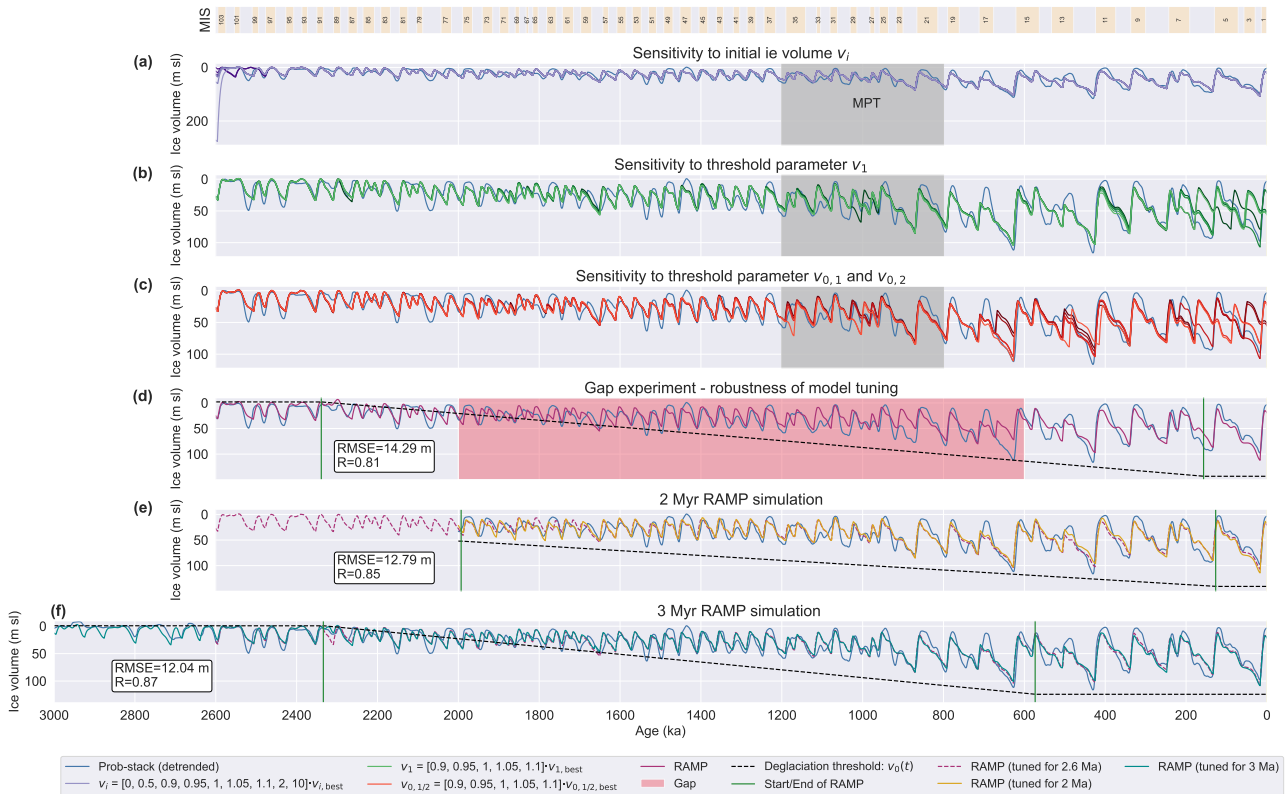
Figure 4. Parameter sensitivity in the RAMP model. **(a)** Sensitivity to initial ~~conditions~~ice volume: v_i ~~(initial quantity)~~ is varied within $[0, 0.5, 0.9, 0.95, 1, 1.05, 1.1, 2, 10] \cdot v_{i,\text{best}}$ (purple lines). **(b)** Sensitivity to model threshold: v_1 is varied within $[0.9, 0.95, 1, 1.05, 1.1] \cdot v_{1,\text{best}}$ (green lines). **(c)** Sensitivity to model thresholds: $v_{0,1}$ and $v_{0,2}$ are simultaneously varied within $[0.9, 0.95, 1, 1.05, 1.1] \cdot v_{0,1/2,\text{best}}$ (red lines). **(d)** Robustness of the model tuning. The RAMP model (purple line) was tuned for the ~~detrended Prob-stack~~Berends GMSL, starting from a unit vector and excluding the period 2 - 0.6 Ma (red-shaded area) from the tuning target. **(e)** RAMP model when tuned for a 2 Myr run (golden line) compared to the standard 2.6 Myr tuned version (purple dotted line). **(f)** RAMP model when tuned for a 3 Myr run (cyan line) compared to the standard 2.6 Myr tuned version (purple dotted line). The blue line shows the ~~detrended Prob-stack~~Berends GMSL. The grey-shaded area highlights the classical perspective of where the MPT is located in time. MIS boundaries are given according to Lisiecki and Raymo (2005).

(last 600 ka), without any information on the glacial cycles during the gap period. The reconstructed ~~benthic δ^{18}O curve~~ global
325 ice volume closely aligns with the ~~target~~ Berends curve (Fig. 4d). In comparison with the reconstructed curve tuned to the complete target (Fig. 1a), the exclusion of the gap results in a slight reduction of the R value from 0.86 to ~~0.77~~0.81. The indicated ramp period remains extended with ~~an earlier onset at ~ 2.3 Ma (previously ~ 2.2 Ma)and~~ a similar start point at 2339 ka (previously 2291 ka), but an earlier end at ~~~ 800~~157 ka (previously ~~~ 500~~546 ka). Despite lacking any information on the glacial cycles during the gap period (red-shaded area in Fig. 4d), the RAMP model can accurately reconstruct the timings of
330 most glacial terminations. ~~This demonstrates the~~Excluding MIS 16 from the tuning target (it falls within the gap period) leads

13

to a failure in reconstructing its large ice volume extent in the RAMP model. Instead, the first extended ice sheets occur later in the simulation, which is linked to the later endpoint of the ramp. Despite MIS 16, the RAMP model is demonstrating high robustness of the applied model tuning ~~and the overall robustness~~ with no signs of overfitting. The strong performance of the RAMP model in ~~accurately reconstructing glacial cycleswithout having any prior knowledge about them~~reliably reproducing glacial cycles, despite lacking any prior information about them, is demonstrated by the high correlation (R = 0.81) between the gap-tuned RAMP model and the Berends curve.

Finally, we alter the simulation period to verify the robustness of the glacial patterns and whether the identified ramp period changes. When we tune the RAMP model for a reduced period of 2 Myr to the ~~detrended Prob-stack~~ Berends GMSL and compare it with the 2.6 Myr tuned version of the RAMP model, both curves almost perfectly align for the past 2 Myr (Fig. 4e). The end of the ramp occurs ~~slightly~~ later in the Quaternary ~~(around 400 ka instead of 500~~ at 127 ka (previously 546 ka). The onset of the ramp is bounded to 2 Ma, due to the reduced simulation period. However, the optimal value for the onset ~~($t_1 = 1936$ kyr)~~ lies very close to this upper bound at 1993 ka, indicating that t_1 might exceed this upper bound, as it does for the 2.6 Myr run.

We repeat the same experiment, but for an extended simulation period of 3 Myr (Fig. 4f). Over the past 2.6 Myr, both curves align almost perfectly. Without an upper bound of 2 Ma for t_1, as in the previous simulation, the model tuning finds a very similar pattern for the temporal shape of the ramp for the 3 Myr run and the 2.6 Myr run. The 3 Myr run results in an onset of the ramp at around ~~2.3 Ma (previously 2.2 Ma~~2334 ka (previously 2291 ka) and an end at ~~around 300~~ 573 ka (previously ~~500~~ 546 ka). Hence, altering the simulation period for the RAMP model does not largely affect the simulated glacial patterns, and the long-lasting trend obtained for the ramp is a robust feature for all simulation periods, although the exact duration of the ramp may vary between the simulations.

4   Discussion

4.1   Ramp-like change ~~for GMSL and benthic δ^{18}O targets~~in v_0

Conceptual models like the RAMP model cannot shed light on the underlying physical mechanisms directly (e.g. whether a long-term trend in v_0 is due to regolith removal or a gradual CO_2 decrease, etc.), since they do not include the involved physical or chemical processes directly. However, their strength lies in their capability to investigate the underlying temporal structure of such a change. The advantage of the new ramp formulation is that the RAMP model incorporates multiple scenarios for the temporal change in the deglaciation parameter, particularly all those discussed in Legrain et al. (2023) (ORB, ABR, GARD). By tuning the model to a ~~paleoclimatic~~ GMSL target curve, it selects the most appropriate temporal structure for $v_0(t)$ ~~. For three out of the four targets used in this study(both GMSL curves and the detrended Prob-stack), the RAMP model shows~~ to reconstruct this curve.

In this study, we applied the new RAMP model to two different GMSL curves. Both targets led to a similar pattern, namely a long-lasting increasing trend in $v_0(t)$, which started between ~~2.2 and~~ 2.6 and 2.3 Ma and ended between ~~250~~ 550 - ~~500~~250 ka. Hence, for these targets, the RAMP is not in favour of an abrupt change, a rather short and limited change (e.g. which only

14

lasted during the MPT) or no change in $v_0(t)$, which would correspond to a purely orbitally driven climate. These findings agree with the results of the L23 models, where the authors identified a gradual trend over the entire 2 Myr-long simulation period to be more likely than an abrupt one or a purely orbital one. The strength of the RAMP model is that it gives information about a potential start and end of such a gradual change. The L23 GRAD model was only run for the past 2 Ma, therefore, it does not allow earlier changes in v_0, but the RAMP model reveals that the change in v_0 likely started even before 2 Ma. An alternative approach is presented in Ganopolski (2024), where the author prescribes the change in the critical ice volume parameter v_c (similar to our v_0) with a hyperbolic tangent, which closely resembles the temporal evolution of the regolith-free area as described in Willeit et al. (2019). This shows that the regolith-free scenario can reproduce the MPT, but since it relies on a single prescribed temporal structure for this change in v_c, it gives no information on how likely such a temporal structure is.

The RAMP model challenges the possibility that orbital forcing alone could explain the MPT. Despite the flexibility of using different linear combinations of ~~precession~~ the precession parameter and obliquity (even when including co-precession), tuning the RAMP model did not result in a scenario where $v_0(t)$ remained constant, but always increased over the Quaternary, i.e. implying that an internal change in the system is required to reconstruct the MPT. In contrast, there are recent studies linking the occurrence of the MPT to orbital forcing alone. Ma et al. (2024) introduce the *integral of annual mean insolation anomaly* (IAMIA), which quantifies successive small step-wise insolation changes over a given period of time. The authors show that IAMIA exhibits a large shift around 935 ka, which they hypothesise to have enabled the onset of the MPT. Another recent ~~preprint by Verbitsky and Omta (2025)~~ study by ? discusses the idea that the MPT is due to a delayed relaxation process, which can lead to an abrupt-like jump in the dominant period. This shift in periodicity can be highly sensitive to the initial conditions, and the sensitivity depends on the amplitude of the orbital forcing. Although our model yields a contrasting view, we cannot exclude the possibility that a different orbital parameterization, e.g. IAMIA, could recreate the MPT.

While the RAMP model supports a long-lasting gradual trend in the Earth-climate system, its underlying physical mechanism cannot be directly inferred but just hypothesized since the conceptual modelling approach lacks the physical representation of these mechanisms. Whether a gradual erosion of regolith (Clark and Pollard, 1998; Clark et al., 2006), a gradual decrease in atmospheric CO_2 (Berends et al., 2021b; Scherrenberg et al., 2025), some sea-ice feedback mechanism, a mixture of these (Willeit et al., 2019) or something else, is the underlying mechanism behind this trend, requires a more physics-based model which can explicitly resolve these mechanisms.

~~The hypothesis of a long-term decrease of atmospheric CO_2 concentrations as the cause of the MPT remains difficult to verify since the continuous direct CO_2 records from Antarctic ice cores are currently limited to the past ~ 800 ka (Willeit et al., 2019; Bereiter et al. and beyond that, the discontinuous ice core samples from the Allan Hills Blue Ice area provide only snapshots of direct CO_2 estimates of the last 3 Ma, attached larger uncertainties (Peterson et al., 2024; Yan et al., 2019). CO_2 estimates over the pre-MPT and the MPT worlds can be obtained using indirect proxies inferred from terrestrial and marine archives. For example, CO_2 reconstructions are based on $\delta^{13}C$ from leaf-wax (Yamamoto et al., 2022), from paleosols (Da et al., 2019), or boron isotope-based reconstructions (Chalk et al., 2017; Hönisch et al., 2009). Based on the latter, there appears to be a decrease in minimal CO_2 concentrations during glacial maxima throughout the MPT. However, looking into a recent synthesis compiling~~

all proxy-based paleo CO₂ data (THE CENOZOIC CO2 PROXY INTEGRATION PROJECT (CENCO2PIP) CONSORTIUM, 2023), alternative CO₂ reconstructions suggest different trends. Hence, there is no clear answer yet regarding the long-term evolution of the atmospheric CO₂ concentration across the Pleistocene. However, this knowledge gap is anticipated to be addressed in the future through ongoing efforts to retrieve a continuous ice core record extending beyond one million years, as pursued, for instance, by the European Beyond EPICA-Oldest Ice Core project and the Australian Million Year Ice Core project.

As Verbitsky and Crucifix (2023) point out, while some phenomenological models can very accurately recreate ~~observational time series(i.e. paleo records)~~ some climatic time series, it does not necessarily reflect their physical similarity to nature. Hence, it is crucial to investigate whether such a ramp-like scenario in the model is justified by paleo records or more sophisticated modelling studies. A synthesis of globally distributed sea surface temperature (SST) records by Clark et al. (2024) found that two long-term cooling stages occurred during the last 4.5 Ma. The first started around 4 Ma, which was followed by a second period of intensified cooling between 1.5 Ma and around 0.8 Ma. Thereafter, temperatures stabilised for the late Pleistocene. A statistical model by Tzedakis et al. (2017) relates glacial terminations with a required energy threshold and shows that this deglaciation threshold had to rise over the Pleistocene. They found that the increase is ramp-like with a linear trend lasting from 1.55 Ma until 0.61 Ma. The conceptual model by Ganopolski (2024) can also recreate the MPT by changing its critical ice volume parameter ramp-like rather than linear. However, it uses a smoother transition function, namely a hyperbolic tangent centered around 1050 ka with a transition time of 250 kyr. The asymptotic behaviour of the hyperbolic tangent leads to quasi-constant parameter values prior to 1.55 Ma (twice the transition time) and after 0.55 Ma. The author stresses the similarity with the modelled regolith mask in Willeit et al. (2019), connecting the ramp-like structure with the erosion of the Northern Hemisphere regolith. The optimal volcanic CO₂ outgassing scenario (V2) found in Willeit et al. (2019) resembles a ramp-like structure for the past 2.6 Ma with a decreasing trend of volcanic CO₂ outgassing between around 2.1 Ma and 0.9 Ma.

In summary, certain proxy records and modelling studies support the concept of a ramp-like internal change. Reaching a constant value for $v_0(t)$ in the RAMP model, after a long increasing trend, aligns with findings from SST records (∼0.8 Ma, Clark et al. (2024)), a statistical model of energy thresholds (∼0.6 Ma, Tzedakis et al. (2017)) and with a modelled volcanic CO₂ outgasing scenario (∼0.9 Ma, Willeit et al. (2019)), where stable conditions were reached in the late Quaternary, although the endpoint for the RAMP model (0.25 - ~~0.5~~ 0.55 Ma) occurs later. The volcanic CO₂ outgassing scenario in Willeit et al. (2019) closely resembles the temporal structure in the RAMP model ~~(for Berends GMSL and detrended Prob-stack)~~ with an early onset around 2.1 Ma. On the other hand, the first cooling trend in global SST records appears earlier (4 Ma), and the intensified cooling trend around 1.5 Ma appears later than the one in the RAMP model. Moreover, the ramp-like energy threshold in Tzedakis et al. (2017) also suggests a later start around 1.55 Ma.

4.2   ~~Seawater $\delta^{18}O_{sw}$~~ Model extrapolation

~~Besides the detrended benthic $\delta^{18}O$ Prob-stack, its deconvolution into seawater $\delta^{18}O_{sw}$ is included in the RAMP model as a new target. This recent deconvolution by Clark et al. (2025b), based on an ocean temperature data compilation, gives a contrasting view compared to the Berends and Rohling deconvolutions. It exhibits a decline in $\delta^{18}O_{sw}$ during the MPT, interrupting a previous period of increasing values and showing larger glacial-interglacial amplitudes in the early Quaternary,~~

435 ~~formulation seems to be less suited for this target, as apparent from the selected ramp period (400 - 200 ka). However, a final reconstruction of this $\delta^{18}O_{sw}$ record into a GMSL curve is not yet available.~~

4.3 ~~Next glacial cycle~~

While neglected in many conceptual models, extrapolating the next glacial cycle can be an important tool of model evaluation, since this represents the only time interval in which a model cannot be tuned or fitted onto some existing paleoclimatic target

440 curve <u>and it can reveal model deficiencies</u>. Since the extrapolated curves lack anthropogenic CO_2 emissions, they must be interpreted as baseline experiments of how the glacial cycles would evolve in the absence of anthropogenic impacts. ~~More complex models, coupled to the carbon cycle, project, even without any anthropogenic influence, an unprecedentedly long Holocene, lasting for another 50 kyr (Ganopolski et al., 2016; Talento and Ganopolski, 2021). In contrast, the RAMP model projects for all four tuning targets that the next glacial cycle has already started~~ <u>The RAMP model consistently crosses the next</u>

445 <u>glaciation threshold</u> 6 ~~- 10 ka~~ ~~and will last until around~~ <u>ka, lasting until</u> 64 kyr in the future. ~~In their recent study, investigating the influence of precession and obliquity on glacial interglacial cycles, Barker et al. (2025) estimate that the current interglacial conditions would last for 11 kyr, when obliquity reaches its next minimum and the succeeding glacial would be interrupted in around 66 kyr (again neglecting anthropogenic effects). Other conceptual models similarly predict a contrasting view for the next glaciation~~<u>Some other conceptual models were also extrapolated into the future</u>: Calder (1974) projected ~~a start~~ <u>the</u>

450 <u>next glacial onset</u> 5 ka~~and an end in~~ ~~,~~ <u>lasting until</u> around 119 kyr (see his Fig. 2), Imbrie and Imbrie (1980) estimated a start 6 ka (see their Fig. 7) and Figure 5 in Paillard (2015) reveals that only a large enough glaciation threshold can lead to a prolonged Holocene in the P98 model, while a lower threshold would have terminated the Holocene already a few kyr ago. While other models like the L23 models ~~, Model 3 of Ganopolski (2024)~~ and the Leloup and Paillard (2022) model were not extrapolated for the next glacial cycle, it can be expected that they would yield similar results as the RAMP model

455 (i.e. a short Holocene), since they are based on similar model dynamics. ~~Therefore, the RAMP characteristic of simulating a prolonged Holocene is a striking feature which is also present in other conceptual models or studies. The discrepancy with the more sophisticated models~~~~might be due to the missing carbon feedback in these models or due to the choice of the glaciation threshold in the RAMP model, which only depends on orbital forcing or parameters~~<u>In their recent study, investigating the influence of precession and obliquity on glacial interglacial cycles, Barker et al. (2025) estimate that the current interglacial</u>

460 <u>conditions would last for 11 kyr, when obliquity reaches its next minimum and the succeeding glacial would be interrupted in around 66 kyr (again neglecting anthropogenic effects).</u>

<u>These results do not agree with more complex models, coupled to the carbon cycle, which project, even without any anthropogenic influence, an unprecedentedly long Holocene, lasting for another 50 kyr (Ganopolski et al., 2016; Talento and Ganopolski, 2021). Hence, the short Holocene, the crossing of the next glacial threshold 6 ka and the failure in stimulating the Holocene minimum</u>

465 <u>in global ice volume do not align with these more complex models. These deficiencies stem from the model design, which does not recognize interglacial states as stable states in the model and yields quick deglaciations followed by long-lasting glaciations.</u>

This becomes apparent from the model equations: In the late Pleistocene, when large ice volume is present, the term $\frac{v(t)}{\tau_d}$ (Eq. 5) dominates the deglaciation regime and leads to very quick removal of the large ice sheets. Hence, the next glaciation threshold $v(t) \cdot \tilde{I}(t) < v_1$ (Eq. 7) is rapidly crossed in the model, leading to a short interglacial state, which is immediately followed by an increase in global ice volume (Eq. 4). Hence, by its very design, the RAMP model cannot produce extended interglacial states and will instead rapidly transition to the next glaciation. This model limitation could be addressed in a future study, either by modifying the threshold equations or by adjusting the differential equation in the deglaciation regime in such a way that it also allows for stable interglacial conditions, instead of just for rapid ice loss.

4.3 Role of precession and obliquity

While we cannot directly investigate the physical effects of precession and obliquity in the climate system with the RAMP model, we can investigate their influence on the dynamics of the model. By using a linear combination of ~~precession~~ the precession parameter and obliquity rather than a single insolation metric, we can explicitly see which roles these two orbital quantities play in the model. For instance, this allows us to investigate the spectral power of the obtained orbital forcing in the RAMP model.

The evolution of the ~~quantity~~ global ice volume $v(t)$ in the RAMP model is driven by a linear combination of ~~two orbital parameters: precession~~ the precession parameter and obliquity, weighted by the model parameters α_{Esi} and ~~obliquity~~ α_{O}. Therefore, the orbital forcing in the model depends on the tuned ~~parameter values α_{Esi} and α_{O}. In comparison~~ values of these two parameters. Compared to other conceptual models, which rely on a specific insolation metric for the orbital forcing (e.g. Ganopolski (2024); Paillard (1998); Leloup and Paillard (2022)), this allows for more flexibility in the model and reduces subjective modelling choices. A similar approach with three orbital parameters has been successfully used in other models (Imbrie et al., 2011; Legrain et al., 2023). Choosing a specific insolation metric does affect the quality of the reconstruction result due to variations in their spectral profiles (Leloup and Paillard, 2022). For instance, the insolation at summer solstice at 65° N has a stronger precession signal than the one obtained from the caloric summer insolation at 65° N (as introduced by Milankovitch (1941)).

Moreover, since using a linear combination of ~~precession~~ the precession parameter and obliquity can accurately reconstruct various insolation curves at different latitudes and seasons (SI Sec. 4), the tuning process will select an optimal curve for the orbital forcing. This optimal forcing curve can then be compared to real insolation curves. In addition, available conceptual models use a variety of orbital forcings, e.g. Model 3 (Ganopolski, 2024) uses the maximum summer insolation at 65° N, P98 relies on the same metric, but with an artificial truncation function added, Tzedakis et al. (2017) use the caloric summer insolation at 65° N. Regarding this variety of different orbital forcings in use, it is of interest to see which metric the RAMP model selects. For the RAMP model, we found that the tuned orbital weights $(\alpha_{\mathrm{Esi}}, \alpha_{\mathrm{O}})$ are almost the same for ~~all four tuning targets~~ both target curves and hence are the orbital forcings $I(t)$. ~~For all four targets, we~~ We find that the curve with the highest correlation ($\cancel{R \geq 0.998}$ $R = 0.999$) is the ISI above a threshold ~~ranging from 339 to~~ of 347 W m^{-2} ~~, at latitudes between~~ at 51° ~~and~~ N for the Berends curve and the ISI above a threshold of 340 W m^{-2} at 53° N for the Rohling curve. These curves consist of a dominant obliquity peak and substantial precessional signals. This contrasts with the widely used insolation curve

18

at summer solstice at 65° N, which exhibits dominant precession signals and a reduced obliquity signal. However, it therefore better resembles the precession-obliquity imprint of the caloric summer insolation curve.

4.4 Model limitations

The RAMP model depends on a specific threshold choice to switch between a glaciation and a deglaciation state. Köhler and van de Wal (2020) challenge this binary view of interglacials and glacials. By classifying interglacials based on the absence of substantial NH land ice outside of Greenland, they found that the classification of interglacials, especially in the early Quaternary, is ambiguous. This classification depends on the defined threshold and the choice of the underlying ~~record~~target curve. This perspective questions the ability of any threshold-based, two-state model to unambiguously classify interglacial states. Therefore, the identified glacial and deglacial states in our model should only be carefully considered in combination with the applied thresholds, defined in Eq. 6,7, and for the used target ~~record (benthic δ^{18}O, sea-water δ^{18}O or global ice volume)~~curve.

Available global mean sea level ~~data~~ reconstructions exhibit large uncertainties. Between 50 and 30 ka, geological and geochemical reconstructions of GMSL vary up to 60 m and above (Farmer et al., 2023). Model-based deconvolutions of global δ^{18}O into GMSL, like for the Berends et al. (2021) and Rohling et al. (2022) sea level reconstructions, exhibit similar large uncertainties. While the Berends curve shows an ~~LGM~~ Last Glacial Maximum (LGM) lowstand of around 100 m, the Rohling curve gives around 108 m. Both values are well below observational-based reconstructions of around 130 - 135 m for the LGM (Austermann et al., 2013; Lambeck et al., 2014; Yokoyama et al., 2000). Furthermore, the Berends and Rohling reconstructions, although differing in their modelling approaches, both rely on the LR04 benthic δ^{18}O stack, whose age model was orbitally tuned. Hence, the chosen reconstruction depends on the orbital tuning applied to the LR04 stack. Consequently, the simulated global ice volume in the RAMP model has to be interpreted in light of the large uncertainties already present in the target data.

Our findings are constrained not only by the uncertainties in the Berends and Rohling GMSL reconstructions but also by the specific choice of which GMSL curve to use as the target for our model, given that there are currently two contrasting interpretations of how global ice volume evolved throughout the Pleistocene. One common approach to disentangle the effects of $\delta^{18}O_T$ and $\delta^{18}O_{sw}$ from benthic foraminifera $\delta^{18}O_b$ is to apply some kind of regression method on $\delta^{18}O_b$ to reconstruct the global ice volume (Berends et al., 2021a; Rohling et al., 2022). This approach reproduces the variability of the underlying $\delta^{18}O_b$ record. In the case of the global $\delta^{18}O_b$ stacks as LR04 (Lisiecki and Raymo, 2005) or Prob-stack (Ahn et al., 2017), this method leads to an increase in global ice volume over the Pleistocene in addition to the shift in frequency. Hence, GMSL reconstructions (and hence global ice volume), as the ones of Berends et al. (2021a) or Rohling et al. (2022), exhibit small global ice volume during the early Pleistocene. This is in contrast with evidence for large NH ice sheet extents already in the early Pleistocene. For instance, Balco and Rovey (2010) found terrestrial evidence of the Laurentide Ice Sheet (LIS) reaching 39° N at 2.4 Ma and 1.3 Ma, Shakun et al. (2016) found similarly large extents of the LIS to mid-latitudes between 2.55 - 1.7 Ma by using a marine $\delta^{18}O_{sw}$ record and Rea et al. (2018) used a multi proxy data set to infer the existence of extended ice sheets grounded within the North Sea, south of ∼60° N from 2.53 Ma. Hence, the Berends and Rohling GMSL reconstructions, as well as similar regression-based reconstructions, do not capture these large ice sheets around ∼2.5 Ma. An alternative approach

is presented in a most recent work by Clark et al. (2025b), where the authors deconvolved the Prob-stack (Ahn et al., 2017) into its seawater $\delta^{18}O_{sw}$ component, based on ocean temperature data. The Prob-stack was corrected for a long-term increase in $\delta^{18}O_b$, possibly due to a combined effect of diagenesis and the carbonate ion effect. This new $\delta^{18}O_{sw}$ record was then subsequently used in Clark et al. (2025a) to reconstruct the GMSL over the past 4.5 Ma by applying a mass-balance approach, considering time-varying temperature and ice volume effects on the $\delta^{18}O$ of ice sheets. They find a sea level lowstand of -151±25 m at 2.52 Ma, which is comparable in size to the LGM lowstand, which aligns with terrestrial and marine evidence for large NH ice sheets during this period, as mentioned above. The extended ice sheets prevail in their reconstruction throughout the entire Pleistocene. Therefore, the new Clark GMSL curve differs fundamentally from former GMSL reconstructions by no longer exhibiting an increase in ice volume over the Pleistocene, but just a shift in glacial frequency. This leaves us with two contrasting views on the evolution of the global ice volume over the MPT. In this study, we selected the Berends and Rohling GMSL curves as target curves instead of the newly published Clark GMSL. This has the following reason: the RAMP model is based on former models (P98, L23), which were specifically designed to simulate an increase in ice volume through an increasing v_0 parameter, hence, the RAMP model is adapted to reconstruct GMSL curves which do show an increasing trend in global ice volume. So, by its model design, the RAMP model is not suited for a GMSL curve as the one presented by Clark et al. (2025a), since this data set no longer exhibits an increase in ice volume. However, we tested various approaches to adjust the RAMP model to simultaneously reconstruct the structurally different Berends and Clark GMSL curves. It seems that an adjustment of the glaciation threshold in combination with a ramp-like change in these threshold parameters is needed. We present this adjusted model, which we call RAMP-2, in the SI (SI Sec. 7). However, further tests are needed to verify the performance of the RAMP-2 model. Thus, leaving us with the RAMP model, applied to the Berends and Rohling GMSL reconstructions. Since the RAMP model is only applicable to a subset of the available GMSL curves, namely the ones which do show an increase in global ice volume, our finding that a long-lasting trend in the deglaciation parameter is key in reproducing the MPT, is limited to these types of GMSL curves and this specific interpretation of the MPT.

5 Conclusions and outlook

In this study, we constructed a new conceptual model of the Quaternary global ~~climate~~ice volume, the so-called RAMP model. It improves the previous L23 models of Legrain et al. (2023) by reducing the ~~number of parameters in the model (2-4 less), reducing the~~ model-data mismatch (ΔRMSE > 1 m), ~~including three new paleo records as target (Rohling GMSL, $\delta^{18}O_b$, $\delta^{18}O_{sw}$),~~ increasing the numerical efficiency (speedup of ~30), refining the tuning strategy, extrapolating the model for the next glacial cycle, testing the model on another target curve, and implementing a more flexible ramp-like parameterization, which includes all former L23 temporal scenarios. Meanwhile, the required number of model parameters has been reduced by two to four. The model is insensitive to ~~the~~ its initial conditions, i.e. the initial ~~value of $v(t)$~~ice volume v_i. While the early Quaternary cycles are less sensitive to changes in the threshold parameters ($v_{0,1/2}, v_1$), the late Quaternary ones are more sensitive, particularly the appearance of interglacial double peaks around MIS 13 and MIS 7. The model tuning is very robust and can yield consistently good results, even when large parts of the tuning targets are excluded, indicating no signs of

overfitting. Reducing or extending the simulation period does not largely affect the simulated glacial cycles, and the identified long-term change in the deglaciation parameter is a very robust feature in the model, although the timing for the onset and end
570   of the ramp varies.

The RAMP model yields consistent results for ~~three tuning targets (Berends GMSL, $\delta^{18}O_b$, $\delta^{18}O_{sw}$). They all~~ both tested GMSL curves (Berends and Rohling). Both result in a long-lasting increasing trend in the deglaciation parameter v_0, which started in the early Quaternary (2.6 - ~~2.2~~ 2.3 Ma) and lasted until ~~250~~ 550 - ~~500~~ 250 ka, in order to reconstruct the MPT. The ~~model fails in reconstructing the recent deconvolution of the Prob-stack into $\delta^{18}O_{sw}$, which fundamentally differs from prior~~
575   ~~deconvolutions. The~~ RAMP consistently projects a short Holocene ~~, which already ended a few kyr ago~~ by crossing the next glaciation threshold 6 ka, followed by an intermediate strong glacial, lasting until around 64 kyr in the future. ~~For all tuning targets~~ However, it underestimates the Holocene minimum in global ice volume.

Furthermore, the RAMP model ~~consistently~~ selects a very similar orbital forcing curve for both GMSL targets, which is in close agreement with the ISI above a threshold ~~ranging from 339 to~~ of 347 W m^{-2} ~~, at latitudes between~~ at 51° ~~and~~ N for the
580   Berends curve and the ISI above a threshold of 340 W m^{-2} at 53° N ~~, which are all characterized~~ for the Rohling curve. Both curves are characterised by a dominant obliquity peak and substantial precession signals. This pattern more closely matches the caloric summer insolation than the insolation at summer solstice at 65° N.

~~At the moment, the RAMP model only relies on precession~~ The RAMP model uses only the precession parameter and obliquity as ~~an input, and it reconstructs either GMSL or $\delta^{18}O$ over~~ inputs, along with a time-dependent v_0 parameter, to
585   reconstruct global ice volume throughout the Quaternary. Internal feedback mechanisms and forcings are conceptualized by aggregated model parameters. ~~This limits the physical interpretability of potential mechanisms driving the climate evolution. Hence, it would be beneficial to include other climatic variables in future work, e.g. CO_2. This would allow us to reconstruct the past evolution of them and improve the physical interpretability of the modelled results.~~ The early onset of the ramp-like change emphasizes the importance of intensifying the work to obtain an even older continuous ice core record than the recently
590   drilled at least ~ 1.2 Ma old ice from the European Beyond EPICA-Oldest Ice Core project to shed further light on the MPT.

Author contributions. F.Po. and F.Pa. designed the conceptual model; F.Po. ran the simulations with the help of F.Pa.; Analysis performed
595   by F.Po., with inputs from F.Pa., E.C., Z.C. and L.J.; F.Po. wrote a draft of the paper, with subsequent inputs from F.Pa., E.C., Z.C., L.J. and E.L.

References

Ahn, S., Khider, D., Lisiecki, L. E., and Lawrence, C. E.: A probabilistic Pliocene–Pleistocene stack of benthic δ18O using a profile hidden Markov model, Dynamics and Statistics of the Climate System, 2, dzx002, https://doi.org/10.1093/climsys/dzx002, 2017.

Austermann, J., Mitrovica, J. X., Latychev, K., and Milne, G. A.: Barbados-based estimate of ice volume at Last Glacial Maximum affected by subducted plate, Nature Geoscience, 6, 553–557, https://doi.org/10.1038/ngeo1859, publisher: Nature Publishing Group, 2013.

Balco, G. and Rovey, II, C. W.: Absolute chronology for major Pleistocene advances of the Laurentide Ice Sheet, Geology, 38, 795–798, https://doi.org/10.1130/G30946.1, 2010.

Barker, S. and Knorr, G.: A Systematic Role for Extreme Ocean-Atmosphere Oscillations in the Development of Glacial Conditions Since the Mid Pleistocene Transition, Paleoceanography and Paleoclimatology, 38, e2023PA004 690, https://doi.org/10.1029/2023PA004690, _eprint: https://onlinelibrary.wiley.com/doi/pdf/10.1029/2023PA004690, 2023.

Barker, S., Starr, A., van der Lubbe, J., Doughty, A., Knorr, G., Conn, S., Lordsmith, S., Owen, L., Nederbragt, A., Hemming, S., Hall, I., Levay, L., and IODP EXP 361 SHIPBOARD SCIENTIFIC PARTY: Persistent influence of precession on northern ice sheet variability since the early Pleistocene, Science, 376, 961–967, https://doi.org/10.1126/science.abm4033, publisher: American Association for the Advancement of Science, 2022.

Barker, S., Lisiecki, L. E., Knorr, G., Nuber, S., and Tzedakis, P. C.: Distinct roles for precession, obliquity, and eccentricity in Pleistocene 100-kyr glacial cycles, Science, 387, eadp3491, https://doi.org/10.1126/science.adp3491, publisher: American Association for the Advancement of Science, 2025.

Bereiter, B., Eggleston, S., Schmitt, J., Nehrbass-Ahles, C., Stocker, T. F., Fischer, H., Kipfstuhl, S., and Chappellaz, J.: Revision of the EPICA Dome C CO2 record from 800 to 600 kyr before present, Geophysical Research Letters, 42, 542–549, https://doi.org/10.1002/2014GL061957, _eprint: https://onlinelibrary.wiley.com/doi/pdf/10.1002/2014GL061957, 2015.

Berends, C. J., de Boer, B., and van de Wal, R. S. W.: Reconstructing the evolution of ice sheets, sea level, and atmospheric CO_2 during the past 3.6 million years, Climate of the Past, 17, 361–377, https://doi.org/10.5194/cp-17-361-2021, publisher: Copernicus GmbH, 2021a.

Berends, C. J., Köhler, P., Lourens, L. J., and van de Wal, R. S. W.: On the Cause of the Mid-Pleistocene Transition, Reviews of Geophysics, 59, https://doi.org/10.1029/2020RG000727, _eprint: https://onlinelibrary.wiley.com/doi/pdf/10.1029/2020RG000727, 2021b.

Bintanja, R. and van de Wal, R. S. W.: North American ice-sheet dynamics and the onset of 100,000-year glacial cycles, Nature, 454, 869–872, https://doi.org/10.1038/nature07158, publisher: Nature Publishing Group, 2008.

Calder, N.: Arithmetic of ice ages, Nature, 252, 216–218, https://doi.org/10.1038/252216a0, publisher: Nature Publishing Group, 1974.

Chalk, T. B., Hain, M. P., Foster, G. L., Rohling, E. J., Sexton, P. F., Badger, M. P. S., Cherry, S. G., Hasenfratz, A. P., Haug, G. H., Jaccard, S. L., Martínez-García, A., Pälike, H., Pancost, R. D., and Wilson, P. A.: Causes of ice age intensification across the Mid-Pleistocene Transition, Proceedings of the National Academy of Sciences, 114, 13 114–13 119, https://doi.org/10.1073/pnas.1702143114, publisher: Proceedings of the National Academy of Sciences, 2017.

Clark, P. U. and Pollard, D.: Origin of the Middle Pleistocene Transition by ice sheet erosion of regolith, Paleoceanography, 13, 1–9, https://doi.org/10.1029/97PA02660, _eprint: https://onlinelibrary.wiley.com/doi/pdf/10.1029/97PA02660, 1998.

Clark, P. U., Archer, D., Pollard, D., Blum, J. D., Rial, J. A., Brovkin, V., Mix, A. C., Pisias, N. G., and Roy, M.: The middle Pleistocene transition: characteristics, mechanisms, and implications for long-term changes in atmospheric pCO2, Quaternary Science Reviews, 25, 3150–3184, https://doi.org/10.1016/j.quascirev.2006.07.008, 2006.

Clark, P. U., Shakun, J. D., Rosenthal, Y., Köhler, P., and Bartlein, P. J.: Global and regional temperature change over the past 4.5 million years, Science, 383, 884–890, https://doi.org/10.1126/science.adi1908, publisher: American Association for the Advancement of Science, 2024.

Clark, P. U., Shakun, J. D., Rosenthal, Y., Pollard, D., Hostetler, S. W., Köhler, P., Bartlein, P. J., Gregory, J. M., Zhu, C., Schrag, D. P., Liu, Z., and Pisias, N. G.: Global mean sea level over the past 4.5 million years, Science, 390, eadv8389, https://doi.org/10.1126/science.adv8389, publisher: American Association for the Advancement of Science, 2025a.

Clark, P. U., Shakun, J. D., Rosenthal, Y., Zhu, C., Bartlein, P. J., Gregory, J. M., Köhler, P., Liu, Z., and Schrag, D. P.: Mean ocean temperature change and decomposition of the benthic δ^{18}O record over the past 4.5 million years, Climate of the Past, 21, 973–1000, https://doi.org/10.5194/cp-21-973-2025, publisher: Copernicus GmbH, 2025b.

Da, J., Zhang, Y. G., Li, G., Meng, X., and Ji, J.: Low CO2 levels of the entire Pleistocene epoch, Nature Communications, 10, 4342, https://doi.org/10.1038/s41467-019-12357-5, publisher: Nature Publishing Group, 2019.

Elderfield, H., Ferretti, P., Greaves, M., Crowhurst, S., McCave, I. N., Hodell, D., and Piotrowski, A. M.: Evolution of Ocean Temperature and Ice Volume Through the Mid-Pleistocene Climate Transition, Science, 337, 704–709, https://doi.org/10.1126/science.1221294, publisher: American Association for the Advancement of Science, 2012.

Farmer, J. R., Pico, T., Underwood, O. M., Cleveland Stout, R., Granger, J., Cronin, T. M., Fripiat, F., Martínez-García, A., Haug, G. H., and Sigman, D. M.: The Bering Strait was flooded 10,000 years before the Last Glacial Maximum, Proceedings of the National Academy of Sciences, 120, e2206742119, https://doi.org/10.1073/pnas.2206742119, publisher: Proceedings of the National Academy of Sciences, 2023.

Ganopolski, A.: Toward generalized Milankovitch theory (GMT), Climate of the Past, 20, 151–185, https://doi.org/10.5194/cp-20-151-2024, publisher: Copernicus GmbH, 2024.

Ganopolski, A., Winkelmann, R., and Schellnhuber, H. J.: Critical insolation–CO2 relation for diagnosing past and future glacial inception, Nature, 529, 200–203, https://doi.org/10.1038/nature16494, publisher: Nature Publishing Group, 2016.

Gildor, H. and Tziperman, E.: A sea ice climate switch mechanism for the 100-kyr glacial cycles, Journal of Geophysical Research: Oceans, 106, 9117–9133, https://doi.org/10.1029/1999JC000120, _eprint: https://onlinelibrary.wiley.com/doi/pdf/10.1029/1999JC000120, 2001.

Gregoire, L. J., Payne, A. J., and Valdes, P. J.: Deglacial rapid sea level rises caused by ice-sheet saddle collapses, Nature, 487, 219–222, https://doi.org/10.1038/nature11257, publisher: Nature Publishing Group, 2012.

Hays, J. D., Imbrie, J., and Shackleton, N. J.: Variations in the Earth's Orbit: Pacemaker of the Ice Ages, Science, 194, 1121–1132, https://www.jstor.org/stable/1743620, publisher: American Association for the Advancement of Science, 1976.

Huybers, P.: Early Pleistocene Glacial Cycles and the Integrated Summer Insolation Forcing, Science, 313, 508–511, https://doi.org/10.1126/science.1125249, publisher: American Association for the Advancement of Science, 2006.

Hönisch, B., Hemming, N. G., Archer, D., Siddall, M., and McManus, J. F.: Atmospheric Carbon Dioxide Concentration across the Mid-Pleistocene Transition, Science, 324, 1551–1554, https://www.jstor.org/stable/20494191, publisher: American Association for the Advancement of Science, 2009.

Imbrie, J. and Imbrie, J. Z.: Modeling the Climatic Response to Orbital Variations, Science, 207, 943–953, https://doi.org/10.1126/science.207.4434.943, publisher: American Association for the Advancement of Science, 1980.

Imbrie, J. Z., Imbrie-Moore, A., and Lisiecki, L. E.: A phase-space model for Pleistocene ice volume, Earth and Planetary Science Letters, 307, 94–102, https://doi.org/10.1016/j.epsl.2011.04.018, arXiv:1104.3610 [astro-ph, physics:physics], 2011.

Köhler, P. and van de Wal, R. S. W.: Interglacials of the Quaternary defined by northern hemispheric land ice distribution outside of Greenland, Nature Communications, 11, 5124, https://doi.org/10.1038/s41467-020-18897-5, publisher: Nature Publishing Group, 2020.

685 Lambeck, K., Rouby, H., Purcell, A., Sun, Y., and Sambridge, M.: Sea level and global ice volumes from the Last Glacial Maximum to the Holocene, Proceedings of the National Academy of Sciences, 111, 15 296–15 303, https://doi.org/10.1073/pnas.1411762111, publisher: Proceedings of the National Academy of Sciences, 2014.

Laskar, J., Robutel, P., Joutel, F., Gastineau, M., Correia, A. C. M., and Levrard, B.: A long-term numerical solution for the insolation quantities of the Earth, Astronomy & Astrophysics, 428, 261–285, https://doi.org/10.1051/0004-6361:20041335, publisher: EDP Sciences, 690 2004.

Legrain, E., Parrenin, F., and Capron, E.: A gradual change is more likely to have caused the Mid-Pleistocene Transition than an abrupt event, Communications Earth & Environment, 4, 1–10, https://doi.org/10.1038/s43247-023-00754-0, number: 1 Publisher: Nature Publishing Group, 2023.

Leloup, G. and Paillard, D.: Influence of the choice of insolation forcing on the results of a conceptual glacial cycle model, Climate of the 695 Past, 18, 547–558, https://doi.org/10.5194/cp-18-547-2022, publisher: Copernicus GmbH, 2022.

Lisiecki, L. E. and Raymo, M. E.: A Pliocene-Pleistocene stack of 57 globally distributed benthic $\delta18O$ records, Paleoceanography, 20, https://doi.org/10.1029/2004PA001071, _eprint: https://onlinelibrary.wiley.com/doi/pdf/10.1029/2004PA001071, 2005.

Ma, X., Yang, M., Sun, Y., Dang, H., Ma, W., Tian, J., Jiang, Q., Liu, L., Jin, X., and Jin, Z.: The potential role of insolation in the long-term climate evolution since the early Pleistocene, Global and Planetary Change, 240, 104 526, 700 https://doi.org/10.1016/j.gloplacha.2024.104526, 2024.

Milankovitch, M.: Kanon der Erdbestrahlung und seine Anwendung auf das Eiszeitenproblem, Royal Serbian Academy Special Publication, 133, 1–633, https://cir.nii.ac.jp/crid/1572824499597240704, publisher: Israel Program for Sceientific Translation, U. S. Department of Commerce, 1941.

Paillard, D.: The timing of Pleistocene glaciations from a simple multiple-state climate model, Nature, 391, 378–381, 705 https://doi.org/10.1038/34891, publisher: Nature Publishing Group, 1998.

Paillard, D.: Quaternary glaciations: from observations to theories, Quaternary Science Reviews, 107, 11–24, https://doi.org/10.1016/j.quascirev.2014.10.002, 2015.

Paillard, D. and Parrenin, F.: The Antarctic ice sheet and the triggering of deglaciations, Earth and Planetary Science Letters, 227, 263–271, https://doi.org/10.1016/j.epsl.2004.08.023, 2004.

710 Parrenin, F. and Paillard, D.: Terminations VI and VIII ($\sim$ 530 and $\sim$ 720 kyr BP) tell us the importance of obliquity and precession in the triggering of deglaciations, Climate of the Past, 8, 2031–2037, https://doi.org/10.5194/cp-8-2031-2012, 2012.

Peterson, J. M., Shackleton, S., Higgins, J., Severinghaus, J., Yan, Y., Buizert, C., Kalk, M., Beaudette, R., Hishamunda, V., Carter, A., Kurbatov, A., Epifanio, J., Morgan, J., Bender, M., and Brook, E.: Ice cores from the Allan Hills, Antarctica show relatively stable atmospheric CO_2 and CH_4 levels over the last 3 million years, https://doi.org/10.21203/rs.3.rs-5610566/v1, iSSN: 2693-5015, 2024.

715 Pérez-Montero, S., Alvarez-Solas, J., Swierczek-Jereczek, J., Moreno-Parada, D., Montoya, M., and Robinson, A.: A simple physical model for glacial cycles, EGUsphere, pp. 1–29, https://doi.org/10.5194/egusphere-2024-1842, publisher: Copernicus GmbH, 2024.

Raymo, M. E. and Huybers, P.: Unlocking the mysteries of the ice ages, Nature, 451, 284–285, https://doi.org/10.1038/nature06589, number: 7176 Publisher: Nature Publishing Group, 2008.

Rea, B. R., Newton, A. M. W., Lamb, R. M., Harding, R., Bigg, G. R., Rose, P., Spagnolo, M., Huuse, M., Cater, J. M. L., Archer, S., Buckley, 720 F., Halliyeva, M., Huuse, J., Cornwell, D. G., Brocklehurst, S. H., and Howell, J. A.: Extensive marine-terminating ice sheets in Europe

from 2.5 million years ago, Science Advances, 4, eaar8327, https://doi.org/10.1126/sciadv.aar8327, publisher: American Association for the Advancement of Science, 2018.

Rohling, E. J., Yu, J., Heslop, D., Foster, G. L., Opdyke, B., and Roberts, A. P.: Sea level and deep-sea temperature reconstructions suggest quasi-stable states and critical transitions over the past 40 million years, Science Advances, 7, eabf5326, https://doi.org/10.1126/sciadv.abf5326, publisher: American Association for the Advancement of Science, 2021.

Rohling, E. J., Foster, G. L., Gernon, T. M., Grant, K. M., Heslop, D., Hibbert, F. D., Roberts, A. P., and Yu, J.: Comparison and Synthesis of Sea-Level and Deep-Sea Temperature Variations Over the Past 40 Million Years, Reviews of Geophysics, 60, e2022RG000 775, https://doi.org/10.1029/2022RG000775, _eprint: https://onlinelibrary.wiley.com/doi/pdf/10.1029/2022RG000775, 2022.

Saltzman, B.: Dynamical Paleoclimatology: Generalized Theory of Global Climate Change, Elsevier, ISBN 978-0-08-050483-4, google-Books-ID: Y975LsF3Q_wC, 2001.

Scherrenberg, M. D. W., Berends, C. J., and van de Wal, R. S. W.: CO_2 and summer insolation as drivers for the Mid-Pleistocene Transition, Climate of the Past, 21, 1061–1077, https://doi.org/10.5194/cp-21-1061-2025, publisher: Copernicus GmbH, 2025.

Shakun, J. D., Raymo, M. E., and Lea, D. W.: An early Pleistocene Mg/Ca-δ18O record from the Gulf of Mexico: Evaluating ice sheet size and pacing in the 41-kyr world, Paleoceanography, 31, 1011–1027, https://doi.org/10.1002/2016PA002956, _eprint: https://agupubs.onlinelibrary.wiley.com/doi/pdf/10.1002/2016PA002956, 2016.

Talento, S. and Ganopolski, A.: Reduced-complexity model for the impact of anthropogenic CO_2 emissions on future glacial cycles, Earth System Dynamics, 12, 1275–1293, https://doi.org/10.5194/esd-12-1275-2021, publisher: Copernicus GmbH, 2021.

THE CENOZOIC CO2 PROXY INTEGRATION PROJECT (CENCO2PIP) CONSORTIUM: Toward a Cenozoic history of atmospheric CO2, Science, 382, eadi5177, https://doi.org/10.1126/science.adi5177, publisher: American Association for the Advancement of Science, 2023.

Tzedakis, P. C., Crucifix, M., Mitsui, T., and Wolff, E. W.: A simple rule to determine which insolation cycles lead to interglacials, Nature, 542, 427–432, https://doi.org/10.1038/nature21364, publisher: Nature Publishing Group, 2017.

Verbitsky, M. and Omta, A. W.: Rapid Communication: Middle Pleistocene Transition as a Phenomenon of Orbitally Enabled Sensitivity to Initial Values, EGUsphere, pp. 1–9, https://doi.org/10.5194/egusphere-2025-3334, publisher: Copernicus GmbH, 2025.

Verbitsky, M. Y. and Crucifix, M.: Do phenomenological dynamical paleoclimate models have physical similarity with Nature? Seemingly, not all of them do, Climate of the Past, 19, 1793–1803, https://doi.org/10.5194/cp-19-1793-2023, publisher: Copernicus GmbH, 2023.

Willeit, M., Ganopolski, A., Calov, R., and Brovkin, V.: Mid-Pleistocene transition in glacial cycles explained by declining CO2 and regolith removal, Science Advances, 5, eaav7337, https://doi.org/10.1126/sciadv.aav7337, publisher: American Association for the Advancement of Science, 2019.

Yamamoto, M., Clemens, S. C., Seki, O., Tsuchiya, Y., Huang, Y., O'ishi, R., and Abe-Ouchi, A.: Increased interglacial atmospheric CO2 levels followed the mid-Pleistocene Transition, Nature Geoscience, 15, 307–313, https://doi.org/10.1038/s41561-022-00918-1, publisher: Nature Publishing Group, 2022.

Yan, Y., Bender, M. L., Brook, E. J., Clifford, H. M., Kemeny, P. C., Kurbatov, A. V., Mackay, S., Mayewski, P. A., Ng, J., Severinghaus, J. P., and Higgins, J. A.: Two-million-year-old snapshots of atmospheric gases from Antarctic ice, Nature, 574, 663–666, https://doi.org/10.1038/s41586-019-1692-3, number: 7780 Publisher: Nature Publishing Group, 2019.

Yokoyama, Y., Lambeck, K., De Deckker, P., Johnston, P., and Fifield, L. K.: Timing of the Last Glacial Maximum from observed sea-level minima, Nature, 406, 713–716, https://doi.org/10.1038/35021035, publisher: Nature Publishing Group, 2000.